RESEARCH ARTICLE

Examination of interannual variability of sea surface temperature in the Indian Ocean using the physical decomposition method

Xingrong Chen[1], Yi Cai[1*] and Fangli Qiao[2]

1. National Research Center for Marine Environmental Forecasts, Beijing, 100081, China.
2. The First Institute of Oceanography, State Oceanic Administration, Qingdao, 266061, China.

Abstract: The physical decomposition method suggested by Qian (2012) is used to examine the interannual variability of sea surface temperature (SST) and anomaly (SSTA) in the Indian Ocean (IO) for the period 1945–2003. The monthly mean SSTs taken from the global ocean reanalysis produced by the Simple Ocean Data Assimilation (SODA) are decomposed into four terms. The first term is the zonally averaged monthly climatological SST ($[\overline{T}_t(\varphi)]$), which features relatively warm surface waters in the tropical IO and relatively colder surface waters over the southern IO. This term also has a relatively low SST pool between the Equator and 20°N. The SST at the center of the pool in summer is about 1–2°C lower than in spring and autumn. The second term is the spatially-varying monthly climatological SSTA ($T_t^*(\lambda,\varphi)$), due mainly to the topographic effect and seasonal variation in wind forcing. The values of $T_t^*(\lambda,\varphi)$ are negative over the western coastal waters and positive over the eastern coastal and shelf waters in the tropical and northern IO. The third term is the zonally-averaged transient SSTA ($[T(\varphi,t)']_Y$). The largest values of $[T(\varphi,t)']_Y$ occur over the subtropical and mid-latitudes of the IO, which differs from the SSTA in the tropical waters of the Pacific Ocean. Time series of zonally and meridionally averaged $T(\varphi,t)'_Y$ in the tropical-subtropical IO is strongly correlated with the Indian Ocean basin-wide (IOBW) mode. The fourth term is the spatially-varying transient SSTA ($T(\lambda,\varphi,t)^{*\prime}_Y$). The REOF analysis of the fourth term demonstrates that the first REOF is correlated strongly with the South Indian Ocean Dipole (SIOD) mode. The second REOF is correlated strongly with the equatorial Indian Ocean dipole (IOD) mode. The third REOF is highly correlated with the tropical IOBW mode.

Keywords: Physical decomposition method, Indian Ocean, sea surface temperature, interannual variability, SODAS, rotated empirical orthogonal function, Indian Ocean dipole mode, Indian Ocean basin-wide mode

*Correspondence to: Yi Cai, National Research Center for Marine Environmental Forecasts, Beijing, China. Email: caiy@nmefc.gov.cn

Received: January 10, 2017; Accepted: March 27, 2017; Published Online: April 16, 2017

Citation: Xingrong Chen, Yi Cai and Fangli Qiao, (2017). Examination of interannual variability of sea surface temperature in the Indian Ocean using the physical decomposition Method. *Satellite Oceanography and Meteorology*, vol.2(1): 49–59. http://dx.doi.org/10.18063/SOM.2017.01.005.

1. Introduction

The Indian Ocean (IO) is the smallest but dynamically complicated among the world's three major oceans (i.e., the Pacific, Atlantic and Indian Oceans). The IO is also the warmest among these three major oceans, with continuous warming of about 0.7–1.2°C during 1901–2012 (Roxy *et al*, 2015). The main physical processes responsible for this century-long warming, however, remain to be fully understood (Saji and Yamagata, 2003; Roxy *et al*, 2014).

The IO plays a very important role in affecting the regional climate variability such as the temporal and spatial variability of the Asian monsoon (Annamalai and Murtugudde, 2004). The temporal and spatial variability of the SST in the IO was suggested to play a very important role in the global climate variability (Abram *et al*, 2008; Chu *et al*, 2014).The rapid warming in the IO was also suggested to be partially responsible for a significant decrease of up to 20% in phytoplankton in this region over the past six decades (Roxy *et al*, 2016).

Circulation and hydrography in the IO also have significant seasonal and interannual variability. The interannual variability of the SST in the IO were studied previously based on observations and numerical simulations (Wu and Meng, 1998; Saji *et al*, 1999; Meng and Wu, 2000; Cai *et al*, 2005; Yang *et al*, 2007; Cai *et al*, 2008;Chu *et al,* 2014; Zhao *et al*, 2016). Based on observational SST data and three sets of reanalysis data in the IO over the period 1958–1998, Saji *et al*. (1999) examined a pattern of internal variability in the SST anomaly (SSTA) known as the Indian Ocean Dipole (IOD) mode. This IOD mode features anomalously low SSTs off Sumatra and high SSTs in the western IO, with noticeable wind and precipitation anomalies. The IOD mode was found to account for ~12% of the SSTA in the IO (Saji *et al*, 1999). Li *et al*. (2003) studied the origin of the Indian Ocean dipole-zonal (IODZ) mode. They demonstrated that the IODZ is a dynamically coupled atmosphere-ocean mode, of which instability depends on the annual cycle of the basic state. The IODZ was found to have a distinctive evolution characteristic compared to the El Niño, and to be a weakly damped oscillator in the absence of external forcing. Yang *et al*. (2007) investigated a basin-wide warming pattern known as the Indian Ocean Basin-wide (IOBW) mode based on the atmospheric reanalysis dataset produced by the National Centers for Environmental Prediction/National Center for Atmospheric Research (NCEP/NCAR). The IOBW mode is characterized by a basin-wide warming or cooling with about 3-year period. Yang *et al*. (2007) demonstrated that the IOBW mode is the dominant mode of SST variability in the IO and this mode peaks in late winter and persists into the following spring and summer in response to an El Niño. Meyers *et al.* (2007) discussed years of El Niño, La Niña, and interactions with the tropical Indian Ocean. Saji and Yamagata (2003) studied that spatial and temporal characteristics of the IOD mode in SST and surface winds using available observations between 1958 and 1997. Chu *et al*. (2014) investigated future changes (2050–2099) of the IOD and IOBW modes together with mean state and El Niño and Southern Oscillation (ENSO) relationship under the anthropogenic global warming using 20 coupled atmosphere-ocean models. Wang *et al*. (2016) studied that the evolution of IOD and its forcing mechanisms based on the analysis of coupled model simulations that allow or suppress the ENSO mode of variability. Their results indicated that ENSO is not fundamental for the existence of IOD. Zhao *et al*. (2016) examined the relationships between the IOBW and IOD of SSTAs over the tropical IO and ENSO phase transition during the following year for the period 1958–2008 and found that the positive (negative) phases of the IOBW and IOD in the tropical IO are possible contributors to the El Niño (La Niña) decay and phase transition to La Niña (El Niño) about one year later. Liu *et al*. (2016) examined the IOD predictability, measured by the Indian Dipole Mode Index (DMI), at the seasonal time scale using the multiple model ensembles and the recently developed information-based theoretical framework of predictability. Although significant research has been done about the SSTAs in the IO, the interannual and decadal variability in the SSTA in the IO are not well understood and deserve further studies.

In most of previous studies on interannual variability of hydrography, it is common to calculate the climatological mean annual cycle averaged over the study period (30 years or longer) from the original (observed or simulated) fields and then extract annual anomalies from the original fields with the annual cycle removed (Titus *et al*, 2013). If the original fields are the monthly mean fields (such as monthly mean SSTs), the original fields are decomposed into the climatological mean monthly means and anomalies. This kind of decomposition is simple but has a drawback since the decomposition of climatological mean monthly means and associated anomalies is not based on main physical processes responsible for the climate variability.

Qian (2012) suggested an alternative method known as the physical decomposition (PD) method in the study of spatially-varying, time-dependent atmospheric conditions during extreme weather conditions. The key of the PD method is to decompose an atmospheric variable such as temperature, humidity, wind

and potential height, into four terms based on the main physical processes affecting the state variable. These four terms consist of (a) the time-averaged zonal symmetric term, (b) the time-averaged asymmetric term, (c) the planetary-scale transient disturbance term, and (d) the weather-scale transient disturbance term. The PD method has successfully been used in studies of extreme weather events such as the regional persistent drought, heavy rainfall, extreme low air temperatures, and extreme hot weathers (Qian, 2012; Qian and Li, 2012; Qian and Liang, 2012; Qian and Zhang, 2012a, b ; Zhu *et al*, 2012).

The main objective of this study is to use the PD method suggested by Qian (2012) to examine the interannual variability of the SSTs in the IO. We will demonstrate the usefulness of this method in the study of low-frequency variability in the large-scale hydrodynamics in the oceans. The structure of this paper is as follows. Section 2 describes the oceanographic data and the PD method used in this study. Section 3 presents the analysis of interannual variability of the SSTA in the IO using the PD method. Section 4 is a summary and conclusion.

2. Data Sources and Physical Decomposition Method

The oceanographic data used in this paper consist of the monthly mean SSTs from January 1945 to December 2003 in the IO between 28.25°E and 116.25°E and between 76°S and 30°N. The monthly mean SSTs over this study region were extracted from the Simple Ocean Data Assimilation (SODA) reanalysis of ocean climate variability (Carton *et al*, 2000a,b), with a horizontal resolution of is 0.50° by 0.50° and 40 z-levels in the vertical. The SODA reanalysis was constructed using an ocean circulation model based on Geophysical Fluid Dynamics Laboratory MOM2 physics. The ocean circulation model was driven by the surface wind reanalysis produced by the NCEP/NCAR (1948–2004) and the European Center for Medium-Range Weather Forecasts (1958–2001), the monthly mean precipitation flux data of the Global Precipitation Climate Program (GPCP), the sea level heights measured by the satellite sea level altimeter, and the sea surface temperatures measured by the improved infrared Very High Resolution Radiometer (AVHRR). The SODA also used an optimal interpolation data assimilation scheme, which combines numerical model forecasts with various observations including hydrographic profiles, ocean station data, moored temperature and salinity measurements, surface temperature and salinity observations from a variety of instruments (e.g., MBT, XBT, CTD, ARGO), SSTs from night time infrared observations from satellites, and satellite based sea level altimetry. The indices for the IOD, IOBW and South Indian Ocean dipole (SIOD) were taken from the dataset constructed by the National Climate Center of China. (http://cmdp.ncc-cma.net/Monitoring/cn_nino_index.php?product=cn_nino_index_iobw).

The physical decomposition method suggested by Qian (2012) is used to decompose the monthly mean SSTs $(T(\lambda,\varphi,t)_Y)$ (in the IO to four physically meaningful terms:

$$T(\lambda,\varphi,t)_Y = \left[\overline{T_t}(\varphi)\right] + T_t^*(\lambda,\varphi) + \left[T(\varphi,t)\right]'_Y + T(\lambda,\varphi,t)_Y^{*\prime} \quad (1)$$

where t represents a given month varying between January and December, subscript Y represents a given year varying between 1945 and 2003, λ represents the longitude, φ represents the latitude, the overbar represents time mean over the study period (1945–2003), and square brackets represent zonal averaging. The phrase of "zonally averaged" in this study is defined as averaging along a latitude circle (or in the east-west direction) using data points with non-zero water depths over the study region (28.25°E–116.25°E and 76°S–30°N).

The four terms on the right-hand side (RHS) of Equation (1) represent SST responses to different large-scale physical processes in the IO. The first term represents the zonally averaged monthly climatological SST associated with the seasonably-varying solar radiation. The second term represents the spatially-varying monthly climatological SSTA due to the topographic effect and seasonal variation in wind forcing. The third term represents the zonally averaged transient SSTA and we will show later that this term is highly correlated with the IOBW mode. The fourth term represents the spatially-varying transient SSTA.

We follow Qian (2012) and calculate the first term based on

$$\left[\overline{T_t}(\varphi)\right] = \frac{1}{P\times N}\sum_{Y=1}^{Y=P}\sum_{\lambda=1}^{\lambda=N} T(\lambda,\varphi,t)_Y \quad (2)$$

where P is the total number of years during the study period, N is the total number of data points in the longitudinal direction (assuming uniform grid spacing in this direction), λ=1 and λ=N represent respectively

the first and last point in the longitudinal direction at each latitude circle, and t and φ have the same meanings as in Equation (1). It should be noted that only SSTs (or $T(\lambda,\varphi,t)_Y$) at data points with non-zero water depths are used in Equation (2) and following equations. The first term of the decomposition is ,therefore, a function of latitude and climatological months and this term is associated mainly with the solar radiation. The latter has significant seasonal and latitudinal variations as mentioned above.

The second term of the decomposition is calculated based

$$T_t^*(\lambda,\varphi)=\frac{1}{P}\sum_{Y=1}^{Y=P}T(\lambda,\varphi,t)_Y-\left[\overline{T_t}(\varphi)\right] \quad (3)$$

This term depends on longitude, latitude and climatological months and it represents the SSTA affected by local topography and wind forcing.

The third term of the decomposition is calculated based on

$$[T(\varphi,t)]'_Y=\frac{1}{N}\sum_{\lambda=1}^{\lambda=N}T(\lambda,\varphi,t)_Y-[\overline{T_t}(\varphi)] \quad (4)$$

and this term is a function of latitude and time (specific month and year).

Finally, the fourth term of the decomposetion can be calculated based on

$$T(\lambda,\varphi,t)_Y^{*\prime}=$$
$$T(\lambda,\varphi,t)_Y-[\overline{T}(\varphi)]-T_t^*(\lambda,\varphi)-[T(\varphi,t)]'_Y \quad (5)$$

which means that the fourth term is the residual of original data field with the first three terms removed.

3. Results

The physical decomposition method presented in Section 2 is used to examine the interannual and seasonal variability in SSTs in the IO. Figure 1 presents the latitude-month distribution of the first term of the decomposition, which is the zonally averaged monthly climatological SST $[\overline{T_t}(\varphi)]$ in the IO. The distribution of $[\overline{T_t}(\varphi)]$ in the IO is correlated strongly with seasonal variations of the solar radiation in the region, which is characterized by relatively warm surface waters of 20°C–28°C with moderate seasonal variations in the tropical region (between 20°N and 25°S) and relatively colder surface waters of less than 14°C with smaller seasonal variations over the southern region(at latitudes of greater than 40°S).There are relatively large seasonal variations in $[\overline{T_t}(\varphi)]$ over the northern IO between the Equator and 30°N. The 26°C isotherm of $[\overline{T_t}(\varphi)]$ is located at about 20°S in summer months of the Southern Hemisphere, and then gradually moves to the Equator from summer to winter months in the Southern Hemisphere. Figure 1 also shows a pool of relatively low values of $[\overline{T_t}(\varphi)]$ in the northern IO between the Equator and 20°N in summer and winter months, which is due mostly to the local topography and general oceanographic circulation in the region (Qian, 2012).

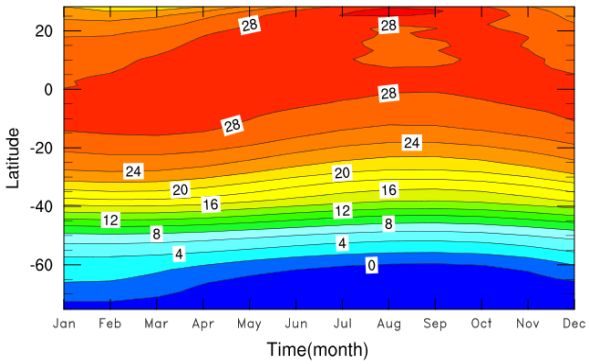

Figure 1. Latitude-month distribution of the zonally averaged monthly climatological sea surface temperature $[\overline{T_t}(\varphi)]$ in the Indian Ocean.

Figure 2 presents spatial distributions of the second term of the physical decomposition (i.e., the spatially-varying monthly climatological SSTA, $T_t^*(\lambda,\varphi)$ in four climatological months of January, April, July and October. Distributions of $T_t^*(\lambda,\varphi)$ in these four months are chosen to represent the seasonal variations of this term. At high latitudes of greater than 45°S in the southern IO, $T_t^*(\lambda,\varphi)$ are negative and similar in these four months, with large negative values over the southern IO centered roughly at 50°S. At mid latitudes between 15°S and 40°S in the IO, distributions of $T_t^*(\lambda,\varphi)$ are characterized by positive anomalies over the western part and negative over the eastern part of the region in these four months. The large-scale wind forcing at high latitudes in the IO is responsible for the above-mentioned distributions of $T_t^*(\lambda,\varphi)$ at the high- and mid-latitudes shown in Figure 2 (Qian and Liang, 2012). Over the northern IO (to the north of 10°S) in these four months, the values of $T_t^*(\lambda,\varphi)$ are negative over the western coastal waters and positive over the eastern coastal and shelf waters. It should be noted that negative values of $T_t^*(\lambda,\varphi)$ over

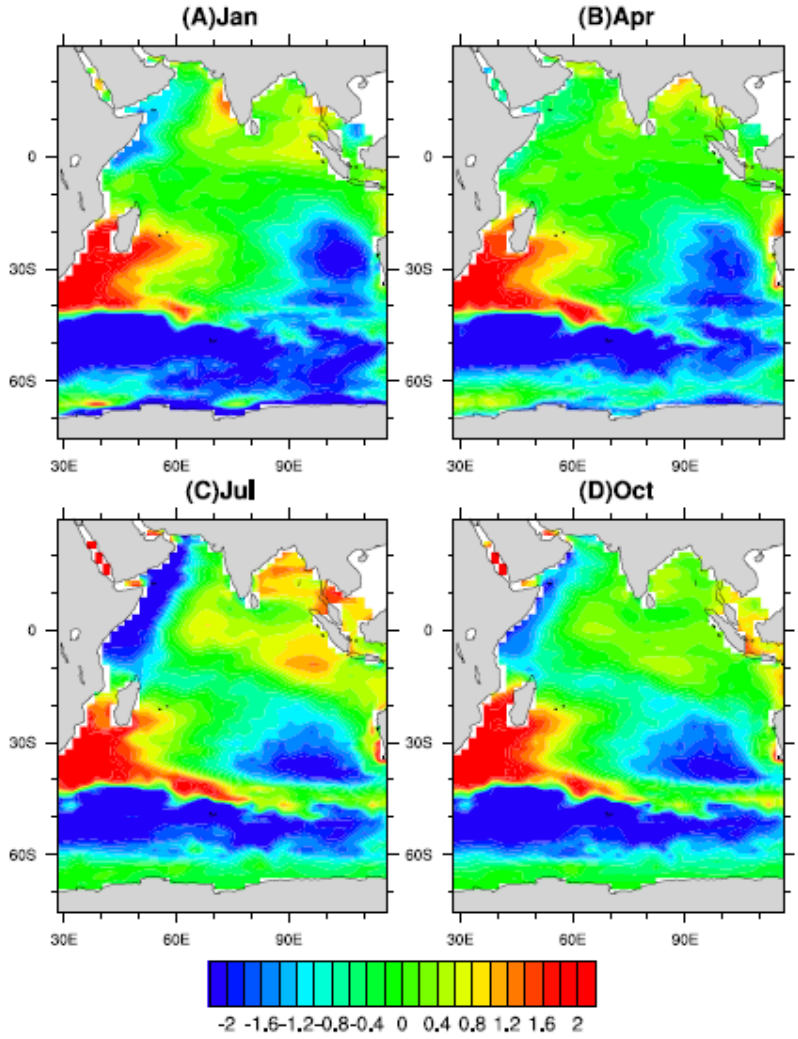

Figure 2. Distributions of monthly climatological sea surface temperature anomaly $T_t^*(\lambda,\varphi)$ in (A) January (B) April, (C) July and (D) October in the Indian Ocean.

the western coastal waters in the northern IO are stronger in summer and autumn months than in winter and spring months (Figure 2). This can be explained by intensive coastal upwelling driven by strong southerly winds in the northern and tropical IO in the summer and autumn seasons. Over the eastern coastal and shelf waters of the northern IO, the positive values of $T_t^*(\lambda,\varphi)$ are associated with the downwelling associated with the southerly winds. In winter and spring seasons, by comparison, relatively small values of $T_t^*(\lambda,\varphi)$ can be explained by relativeely weak wind forcing in the tropical and sub- tropical IO in these two reasons.

Figure 3 presents latitude-month distributions of the third term of the decomposition (the zonally averaged transient SSTA, $[T(\varphi,t)]'_Y$ during the 59-year period between 1945 and 2003. There is significant temporal and meridional variability in $[T(\varphi,t)]'_Y$ in the IO, with indications of propagations of the anomalies in the meridional direction (i.e., the north-south direction). To examine the temporal and meridional variability of these anomalies, the IO is separated from north to south to the tropical/subtropical zone (25°N–25°S, zone A), mid-latitude zone (25°S–45°S, zone B), and mid/high latitude zone (45°S–70°S, zone C). In zone C, the SST anomalies of $[T(\varphi,t)]'_Y$ propagate southward from the mid-latitude zone to high-latitude zone, with propagation periods of about 6 months. The southward propagations of positive anomalies of $[T(\varphi,t)]'_Y$ from mid-latitudes to high-latitudes in zone C occur in years of 1945, 1946, 1947 1948, 1952, 1955, 1956, 1958, 1965, 1966, 1967, 1988, 1989, 1992,

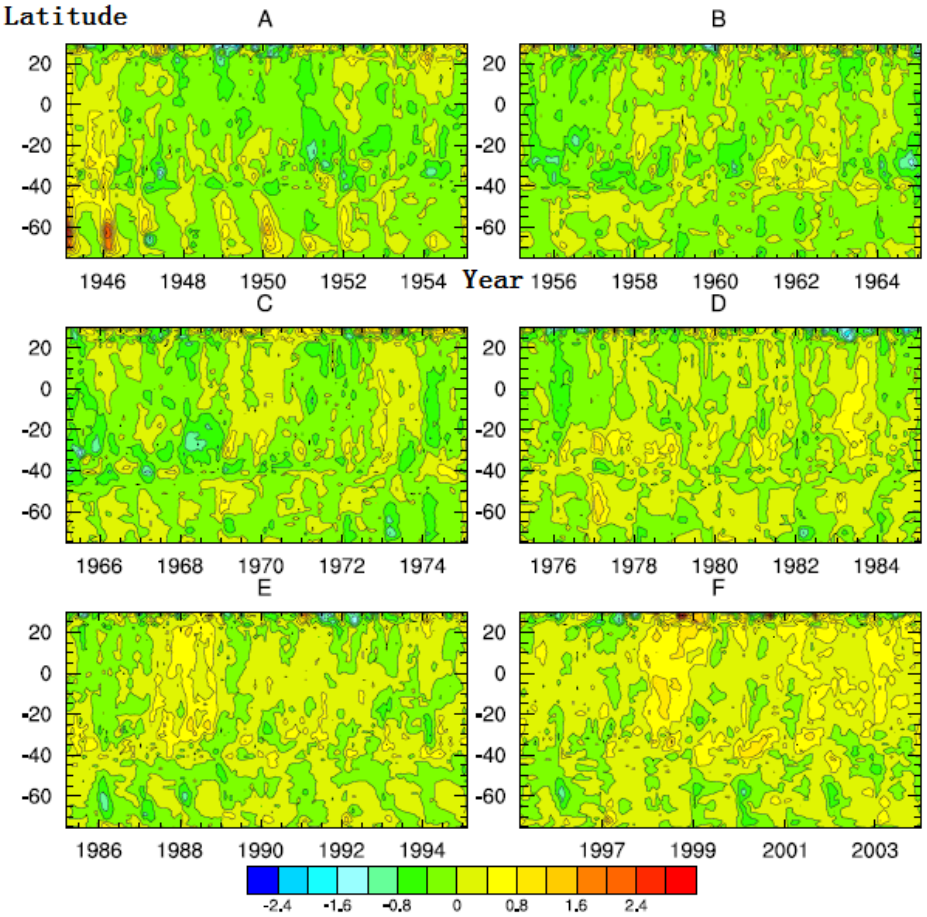

Figure 3. Latitude-year distributions of zonally-averaged transient sea surface temperature anomaly SSTA $T(\varphi,t)'_Y$ in the Indian Ocean in periods (A) 1945−1955, (B) 1955−1965, (C) 1965−1975, (D) 1975−1985, (E) 1985−1995, and (F) 1995-2003.

1994, 1997, and 2003. By comparison, southward propagations of negative anomalies of $[T(\varphi,t)]'_Y$ occur in years 1962, 1973, 1974, 1986, 1988, 1989, 1991, 1993, 1994, 1996, 1999, 2000 and 2002. Furthermore, southward propagations of many positive (negative) anomalies occur before (after) the 1980s.

To determine the dominant frequencies of variabilities in $[T(\varphi,t)]'_Y$ over zone C, the monthly values of zonally averaged transient SSTA are averaged meridionally between 45°S and 70°S to obtain spatially (zonally and meridionally) averaged transient SSTA over this zone defined as $[T(\varphi,t)]'_Y$. The spectral analysis for time series of $[T(\varphi,t)]'_Y$ yields periods of dominant variabilities of about 2, 10 and 30 years for zone C. Over the transition between zones A and B, large temporal variabilities occur in $[T(\varphi,t)]'_Y$, with relatively short periods of about 2–3 years (Figure 3). In zone A, by comparison, positive and negative values of $[T(\varphi,t)]'_Y$ occur alternatively. The spectral analysis of time series of $[T(\varphi,t)]'_Y$ in zone A yields two dominant periods of about 3 and 20 years.

To determine correlation between time series of spatially averaged transient SSTA $[T(\varphi,t)]'_Y$ over different zones in the IO, a cross-correlation analysis is conducted and results are presented in the Table 1. A high correlation occurs in time-series of $[T(\varphi,t)]'_Y$ between zone A (tropical/subtropical IO) and zone B (mid-latitude IO), with the maximum correlation coefficient of~0.65 at the time lag of ~4 months (time series in zone B is leading). The correlation in time series of $[T(\varphi,t)]'_Y$ between zone B (mid-latitude IO) and zone C (mid/high-latitude IO) is also statistically significant, with the maximum correlation coefficient of ~0.37 at the time lag of~72 months (time series in zone B is leading). Therefore, the large variability in the spatially averaged transient SSTA (or $[T(\varphi,t)]'_Y$) at mid-latitudes in the IO (25°S–45°S) propagate both northwards to zone A and southwards to zone C

Table 1. Results of cross-correlation analyses of spatially averaged $[T(\varphi,t)]'_Y$ between different zones in Indian Ocean.

Index	Leading Zone	Lagging Zone	τ (in months)	Maximum R_{xy}
1	Zone C	Zone B	0	0.11
2	Zone B	Zone C	72	0.37
3	Zone B	Zone A	4	0.65
4	Zone A	Zone B	0	0.63
5	Zone A	Zone C	120	0.29
6	Zone C	Zone A	5	0.13

Zone A is the tropical/subtropical region (25°N–25°S). Zone B is the mid-latitude region (25°S–45°S). Zone C is the mid/high latitude region (45°S–70°S). In the table, τ is the time lag at which the cross-correlation coefficient (R_{xy}) is the maximum, and "Leading Zone" and "Lagging Zone" mean zones with the leading and lagging time series in the analyses.

respectively, with northward propagations to zone A to be stronger than the southward propagations to zone C in the IO.

An important question is raised regarding the relationship between the zonally and meridionally averaged transient SSTA $[T(\varphi,t)]'_Y$ and the Indian Ocean dipole (IOD) mode and Indian Ocean basin-wide (IOBW) mode. A cross-correlation analysis indicates that time series of spatially averaged SSTA $[T(\varphi,t)]'_Y$ in zone A (tropical-subtropical IO) is correlated to the IOD mode with the maximum correlation coefficient of~0.42 at the time lag of~6 months (IOD is leading). The time series of $[T(\varphi,t)]'_Y$ in zone B (mid-latitude IO) is also correlated to the south Indian Ocean Dipole (SIOD) mode, with the maximum correlation coefficient of ~0.4 at the time lag of about one year. Therefore, both IOD and SIOD modes play a very important role to the temporal variability of $[T(\varphi,t)]'_Y$ A correlation analysis also indicates that the spatially averaged SSTA $[T(\varphi,t)]'_Y$ in zone A is strongly correlated with the IOBW mode, with the maximum correlation coefficient of ~0.97 at the zero lag. Figure 4 presents time series of $[T(\varphi,t)]'_Y$ in zone A and the IOBW index. Both time series shown in Figure 4 have a warming trend, with significant interannual and decadal variabilities.

We next examine the fourth term of the physical decomposition given in Equation (5), noted as $T(\lambda,\varphi,t)^{*'}_Y$, using the rotating empirical orthogonal function (REOF) analysis. The REOF linearly transforms the spatial patterns derived by the conventional EOF analysis into a rotated basis (Lian and Chen, 2012). The main advantage of the REOF analysis is that it simplifies

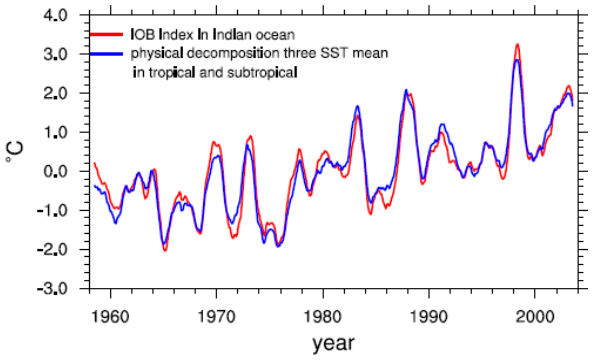

Figure 4. Time series of the Indian Ocean Basin (IOBW) mode index (red) and spatial averaged SSTA $[T(\varphi,t)]'_Y$ in zone A (tropical-subtropical Indian Ocean) (blue) during the period 1950–2003.

spatial structures while retaining the robust patterns (Hannachi *et al*, 2006).

Figure 5A and Figure 6 present respectively the pattern and time-dependent coefficient for the first REOF mode of $T(\lambda,\varphi,t)^{*'}_Y$. This mode accounts for ~4.3% of the total variance of the SSTA in the IO. The spatial distribution of the first REOF mode in the IO is consistent with the typical pattern of the subtropical Indian Ocean Dipole (STIOD). The mode coefficient of the first REOF is correlated significantly with the STIOD index, with the correlation coefficient to be about –0.74 during the period 1958–2003 (Figure 6A). The mode coefficient of the first REOF for $T(\lambda,\varphi,t)^{*'}_Y$ is also highly correlated to the spatially averaged $T(\lambda,\varphi,t)^{*'}_Y$ in the mid-latitude IO (zone B) during the period 1948–2003, with the correlation coefficient of about –0.55 at the time lag of ~13 months (the mode coefficient is leading). Therefore, the first REOF for $T(\lambda,\varphi,t)^{*'}_Y$ in the IO, as well as the spatially averaged $[T(\varphi,t)]'_Y$ in the mid-latitude IO, is caused by the subtropical Indian Ocean dipole (STIOD) rather than the tropical Indian Ocean dipole (IOD), which differs from the counterparts in the Pacific Ocean. It should be noted that the horizontal distribution of the first REOF for the SSTA shown in Figure 5A is similar to the SSTA distribution in the tropical Pacific Ocean, both of which are caused mainly by the wind forcing. For the simplicity of discussion, only the wind forcing in the north-south direction (meridional wind) is considered. Figure 5B presents the spatial pattern of the third REOF for the fourth term of the meridional wind $T(\lambda,\varphi,t)^{*'}_Y$ decomposition in the IO during the period 1948–2003. The third REOF explains

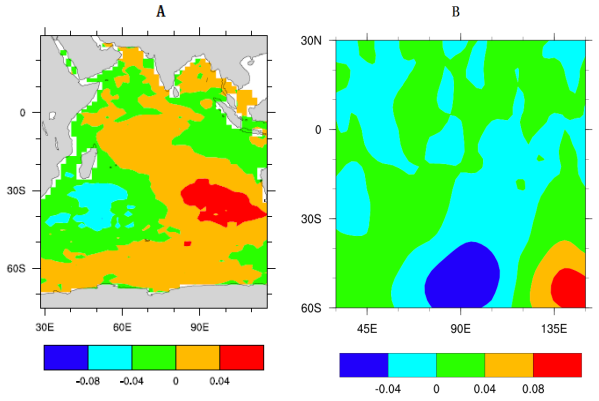

Figure 5. Spatial distributions of (A) the first REOFs for the fourth term of the decomposition $T(\lambda,\varphi,t)_Y^{*\prime}$ and (B) the third REOF for the meridional wind in the Indian Ocean.

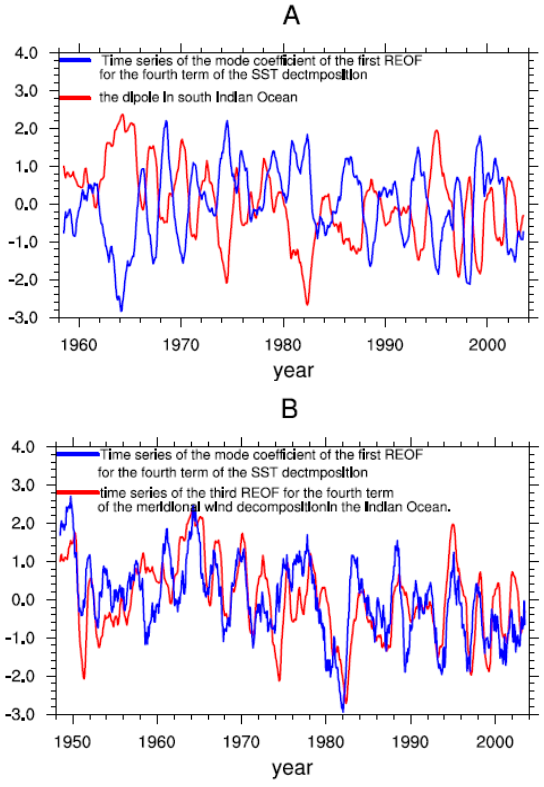

Figure 6. Time series of the mode coefficient (blue) of the first REOF for the fourth term of the decomposition $T(\lambda,\varphi,t)_Y^{*\prime}$. Also shown in (A) time-series of the subtropical Indian Ocean dipole (STIOD, red dashed) and (B) time series of the third REOF for the meridional wind in the Indian Ocean (red).

reasonably well the spatial distribution of the first REOF for $T(\lambda,\varphi,t)_Y^{*\prime}$. A comparison of time series of the first REOF mode coefficient for $T(\lambda,\varphi,t)_Y^{*\prime}$ with time series for the third REOF mode coefficient for the fourth term of the meridional wind $T(\lambda,\varphi,t)_Y^{*\prime}$ decomposition during the period 1948-2003 is shown in Figure 6B. These two-time series are highly correlated, with the correlation coefficient to be ~0.66 (the meridional wind is leading). The main physical explanation for the high correction between the anomalous meridional winds and SSTA in the IO is due to the fact that the direction of Ekman transport in deep waters of the South Hemisphere is 90° to the left-hand side of the wind direction. As a result, the positive SSTA over the eastern region of zone B (mid-latitude IO) shown in Figure 6A can be explained by anomalous downwelling generated by the positive anomalies of meridional winds to the south-east of the positive SSTA (Figure 6B). Similarly, the negative SSTA over the western region of zone B shown in Figure 6A can be explained by anomalous upwelling generated by negative anomalies of meridional winds to the south-east of the negative SSTA.

Figure 7 presents the pattern and mode coefficient of the second REOF for $T(\lambda,\varphi,t)_Y^{*\prime}$ during the period 1945–2003. This component accounts for about 4.0% of the total variance of the SSTA in the IO. The general pattern of the second REOF features a tripole distribution in the southern IO between 15°S and 50°S. The mode coefficient for the second REOF has a linear trend, indicating this mode represents partially the response of the SSTA to the global warming. A correlation analysis indicates that the time-dependent coefficient for the second REOF mode is correlated with the spatially averaged third term of the decomposition in zone A $[T(\varphi,t)'_Y]$, with the correlation coefficient of ~0.38 (the second REOF is lagging). The time-dependent mode coefficient of the second EROF is also correlated with the IOD mode with the correlation coefficient of about –0.3 at the zero lag. Therefore, it can be argued that the second REOF mode represents partially the IOD mode.

Figure 8 presents the pattern and time-dependent mode coefficient of the third REOF for $T(\lambda,\varphi,t)_Y^{*\prime}$. This mode accounts for about 3.4% of total variance of the SSTA in the IO. This mode has more small-scale features than the first two REOF modes as expected. Except for coastal and shelf waters of the eastern and western IO, the third REOF represents the general warming trend over the central IO. The time series of the third REOF is correlated highly with the IOBW mode, with the correlation coefficient of ~0.71 (IOBW is leading).

4. Summary and Conclusion

The physical decomposition (PD) method suggested by

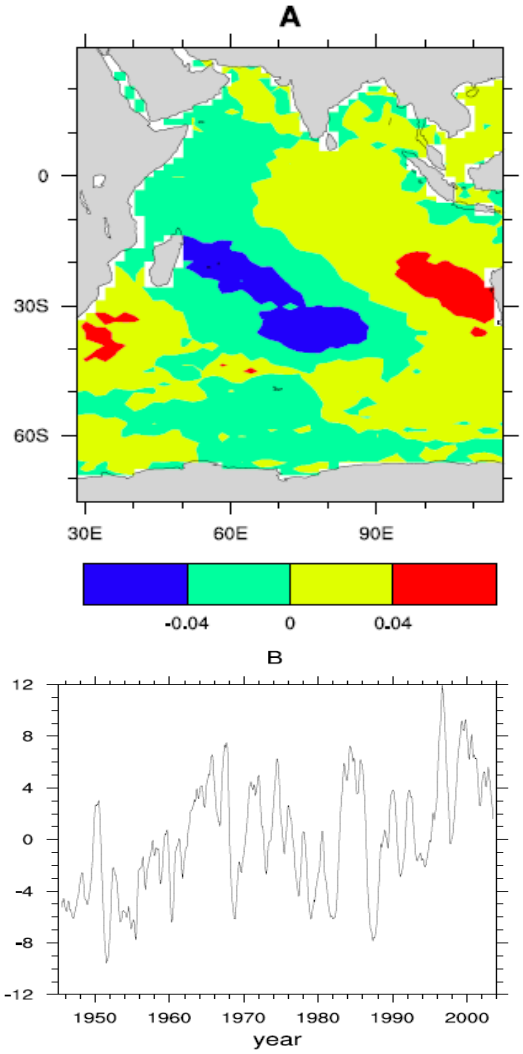

Figure 7. (A) Spatial distribution and (B) time-series of the mode coefficient of the second REOF for the fourth term of the decomposition $T(\lambda,\varphi,t)_Y^{*'}$ in the Indian Ocean.

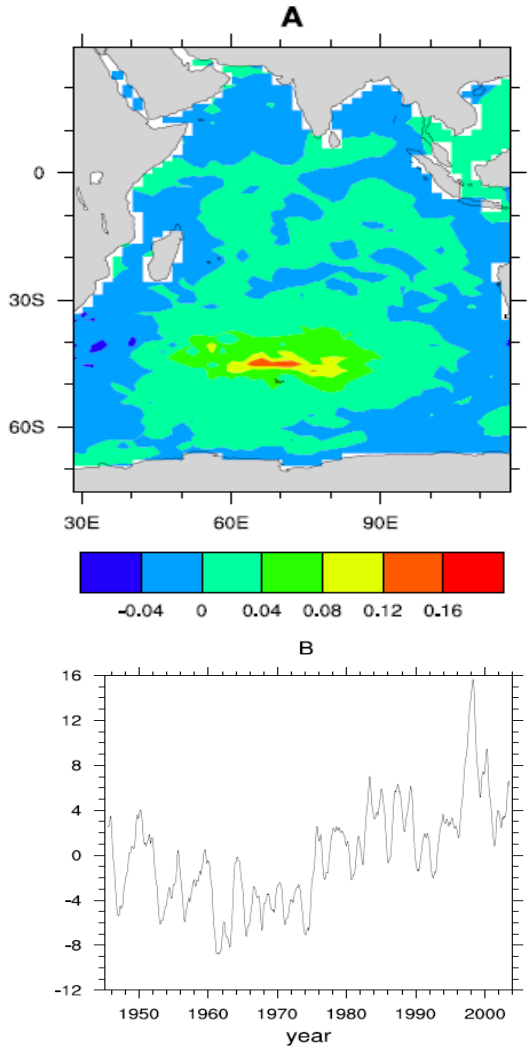

Figure 8. (A) Spatial distribution and (B) time-series of the mode coefficient of the third REOF for the fourth term of the decomposition $T(\lambda,\varphi,t)_Y^{*'}$ in the Indian Ocean.

Qian (2012) was used in this study to examine the temporal and spatial variability of sea surface temperature (SST) and associated anomaly (SSTA) in the Indian Ocean (IO), with a special emphasis of the interannual variability. The monthly mean SST data in the IO were taken from the Simple Ocean Data Assimilation (SODA) reanalysis of ocean climate variability (Carton *et al*, 2000a), with a horizontal resolution of is 0.50° by 0.50° and 40 z-levels in the vertical.

The monthly mean SSTs in the IO were decomposed to four physics-based terms using the PD method. The first term $[\overline{T_t}(\varphi)]$ represents the zonally averaged monthly climatological SST associated with the solar radiation. The second term $T_t^*(\lambda,\varphi)$ represents the spatially-varying monthly climatological SSTA due to the topographic effect and seasonal variation in wind forcing. The third term $[T(\varphi,t)]_Y'$ represents the zonally averaged transient SSTA. The fourth term $T(\lambda,\varphi,t)_Y^{*'}$ represents the spatially-varying transient SSTA.

The zonally averaged monthly climatological SST (the first term $[\overline{T_t}(\varphi)]$) in the IO was found to have relatively warm surface waters of 20°C–28°C with moderate seasonal variations in the tropical region (between 20°N and 25°S) and relatively colder surface waters of less than 14°C with smaller seasonal variations over the southern region(at latitudes of greater than 40°S). This term has relatively smaller seasonal variability in the mid-latitudes (35°S–50°S) than other regions of the IO. This term also features a pool of

relatively lower SST of 1–2°C in summer (July–September) than in spring and autumn over the tropical IO between the Equator and the 20°N.

Due to the effect of coastline and seasonal variability in surface wind forcing, the spatially-varying monthly climatological SSTA (second term: $T_t^*(\lambda,\varphi)$) has significant temporal and spatial variability. In the northern IO between 10°S and 20°N, this term features large positive anomalies over the eastern coastal waters and large negative anomalies over the western coastal waters in summer and autumn. In the other two seasons, the spatial differences in the SSTA are relatively small between the eastern and western coastal waters in the northern IO, due to relatively weaker winds in winter and spring. At mid-latitudes between 15°S and 30°S in the IO, positive values of $T_t^*(\lambda,\varphi)$ occur over the western part and negative values over the eastern part of the region in these four months. At high latitudes of greater than 45°S, distributions of $T_t^*(\lambda,\varphi)$ in these four months are similar and negative, with large negative values over the southwestern IO centered roughly at 45°E and 50°S. The large-scale wind forcing at high latitudes in the IO is responsible for the above-mentioned distributions of $T_t^*(\lambda,\varphi)$ at the high and mid latitudes.

Based on distributions of zonally averaged transient SSTA (the third term: $[T(\varphi,t)]'_Y$), the IO was separated to the tropical/subtropical zone (25°N–25°S, zone A), mid-latitude zone (25°S–45°S, zone B), and mid/high latitude zone (45°S–70°S, zone C). The positive (negative) anomalies of $[T(\varphi,t)]'_Y$ were found to propagate from zone B to zone C before (after) 1980s. It was also found that the largest and most important SSTA in the IO occurred in the subtropical and mid-latitude IO (near 40°S) rather than in the tropical IO, which differ from the occurrence of the largest SSTA in the tropical Pacific Ocean. Furthermore, the zonally and meridionally averaged SSTA $[T(\varphi,t)]'_Y$ in zone A is strongly correlated with the Indian Ocean basin-wide (IOBW) mode, with the maximum correlation coefficient of ~0.97 at the zero lag. The large SSTAs denoted by $[T(\varphi,t)]'_Y$ are correlated with large anomalies in the southerly winds in the mid-latitude IO, with the wind forcing to be leading about 3 months.

The temporal and spatial variability of the fourth term of the decomposition (noted as $T(\lambda,\varphi,t)^{*'}_Y$) was examined using the rotated empirical orthogonal function (REOF) analysis. It was found that the first REOF is correlated strongly with the South Indian Ocean Dipole (SIOD) mode. The second REOF is correlated strongly with the equatorial Indian Ocean dipole mode (IOD). The third REOF is highly correlated with the tropical IOBW mode. The time-dependent coefficients for the second and third REOFs have a significant warming trend.

The PD method was found in this study to be useful in examining the seasonal and interannual variability of the SST and SSTA in the IO. This method was originally developed for the analyses of extreme atmospheric conditions (Qian, 2012). It should be noted that the PD method does not consider the direct effect of coastline. The coastline, however, plays strong constraints in oceanographic conditions much more than in atmospheric conditions. Future studies are needed to include the coastline effect in the physical decomposition method.

Conflict of Interest

No conflict of interest was reported by all authors.

Acknowledgement and Funding

We thank professor Jinyu Sheng for his valuable comments on the early version of this manuscript.

References

Abram N J, Gagan M K, Cole J E *et al*. (2008). Recent intensification of tropical climate variability in the Indian Ocean. *Natural Geoscience*, 1:849–853. http://dx.doi.org/10.1038/ngeo357.

Nerilie J A, Michael K G, Julia E C *et al.* (2008). Recent intensification of tropical climate variability in the Indian Ocean. *Natural Geoscience*, 1:849–853. http://dx.doi.org/10.1038/ngeo357.

Cai Y, Hai L and Zhang R. (2008). The further research on the relationship between tropical Indian Ocean temperature anomaly and ENSO. *Journal of Meteorological Research*, 66(1): 120–124.

Cai Y, Zhang J and Yu W. (2005). The analysis of the upper sea temperature of Equatorial Pacific-Indian ocean. *Journal of Tropical Oceanography*, 24(4): 60–68.

Carton J A, Chepurin G, Cao X *et al*. (2000a). A simple ocean data assimilation analysis of the global upper ocean 1950–95. *Part I: Methodology. Journal of Physical Oceanography*, 30: 294–309. http://dx.doi.org/10.1175/1520-0485(2000)030%3c0294:ASODAA%3e2.0.CO;2.

Carton J A, Chepurin G, Cao X *et al*. (2000b). A simple ocean data assimilation analysis of the global upper ocean 1950–95. *Part II: Results. Journal of Physical Oceanog-*

raphy, 30: 311–326. http://dx.doi.org/10.1175/1520-0485(2000)030%3c0294:ASODAA%3e2.0.CO;2.

Chu J, Ha K, Lee J *et al*. (2014). Future change of the Indian Ocean basin-wide and dipole modesin the CMIP5. *Climate Dynamics*, 43: 535–551. http://dx.doi.org/10.1007/s00382-013-2002-7.

Hannachi A, Jolliffe I T, Stephenson D B *et al*. (2006). In search of simple structures in climate: Simplifying EOFs. *International Journal of Climatology*, 26: 7–28. http://dx.doi.org/10.1002/joc.1243.

Li T, Wang B, Chang C-P *et al*. (2003). A theory for the Indian Ocean Dipole Zonal Mode. *Journal of the Atmospheric Sciences*, 60: 2119–2135. http://dx.doi.org/10.1175/1520-0469(2003)060%3c2119:ATFTIO%3e2.0.CO;2.

Lian T and Chen D. (2012). An Evaluation of Rotated EOF Analysis and Its Application to Tropical Pacific SST Variability. *Journal of Climate*, 8: 5361–5373. http://dx.doi.org/10.1175/JCLI-D-11-00663.1.

Liu H, Tang Y, Chen D *et al*. (2016). Predictability of the Indian Ocean dipole in the coupled models. *Climate Dynamics*, 48(5): 2005–2024. http://dx.doi.org/10.1007/s00382-016-3187-3.

Meng W and Wu G. (2000). The gear coupling of air-sea system of Equatorial Indian-Pacific region and ENSO events II: numerical model simulations. *Atmospheric Science*, 24(1): 15–2.

Meyers L, McIntosh P, Pigot L *et al*. (2007). The years of El Niño, La Niña, and interactions with the tropical Indian Ocean. *Journal of Climate*, 20: 2872–2880. http://dx.doi.org/10.1175/JCLI4152.1.

Qian W. (2012). The physical decomposition principle of regional scale atmospheric transient anomaly. *Chinese Journal of Geophysics*, 55(5):1439–1448.

Qian W and Li J. (2012). The hiatus during the long warming of Beijing. *Advances in Climate Change Research*, 8(3): 178–182.

Qian W and Liang H. (2012). The atmospheric teleconnection patterns in the northern hemisphere and regional-scale atmospheric disturbances. *Chinese Journal of Geophysics*, 55(5): 1449–1461.

Qian W and Zhang Z. (2012a). The early signals of the lasting low temperature and freezing rain forecasting in South. *Chinese Journal of Geophysics*, 55(5): 1501–1512.

Qian W and Liang H. (2012). Propagation of planetary-scale zonal mean wind anomalies and polar oscillations. *Chinese Science Bulletin*, 57: 2606. http://dx.doi.org/10.1007/s11434-012-5168-1.

Qian W and Zhang Z. (2012b). The planetary and synoptic scale disturbance signals of the lasting drought in southwest. *Chinese Journal of Geophysics*, 55(5): 1487–1500.

Roxy M, Ritika K, Terray P *et al*. (2014). The curious case of Indian Ocean warming. *Journal of Climate*, 27: 8501–8509. http://dx.doi.org/10.1175/JCLI-D-14-00471.1.

Roxy M K, Ritika K, Terray P *et al*. (2015), Indian Ocean warming-The bigger picture, Bull. *American Meteorological Society*, 96(7): 1070–1071.

Roxy M K, Modi A, Murutugudde R *et al.* (2016). A reduction in marine primary productivity driven by rapid warming over the tropical Indian Ocean.Geophys. *Research Letter*, 43(2): 826–833. http://dx.doi.org/10.1002/2015gl066979.

Saji N H, Goswami B N, Vinayachandran P N *et al*. (1999). A dipole mode in the tropical Indian Ocean. *Nature*, 401: 360–363.

Saji N H and Yamagata T. (2003). Structure of SST and surface wind variability during Indian Ocean dipole mode events: COADS observations. *Journal of Climate*, 16: 2735–2751. http://dx.doi.org/10.1175/1520-0442(2003)016<2735:SOSASW>2.0.CO;2.

Titus L, Sheng J, Greatbatch R J *et al*. (2013). Improving statistical downscaling of general circulation models. *Atmosphere-Ocean*, 51: 213–225. http://dx.doi.org/10.1080/07055900.2013.774259..

Wang H, Murtugudde R and Kumar A. (2016). Evolution of Indian Ocean dipole and its forcing mechanisms in the absence of ENSO. *Climate Dynamics*, 47: 2481–2500. http://dx.doi.org.10.1007/s00382-016-2977-y.

Wu G and Meng W. (1998). The gear coupling of air-sea system of Equatorial Indian-Pacific region and ENSO events I:data analysis. *Atmospheric Science*, 22(4): 470–480.

Yang J L, Liu Q Y, Xie S-P *et al*.(2007). Impact of the Indian Ocean SST basin mode on the Asian summer monsoon. *Geophysical Research Letters*, 34: L02708. http://dx.doi.org/10.1029/2006GL028571.

Zhao, X, Yuan D, Yang G *et al*. (2016). Role of the oceanic channel in the relationships between the basin/dipole mode of SST anomalies in the tropical Indian Ocean and ENSO transition. *Advances in Atmospheric Sciences*, 33(12): 1386–1400. http://dx.doi.org/10.1007/s00376-016-6048-4.

Zhu C, Bin W, Qian W *et al.* (2012). Recent weakening of northern East Asian summer monsoon: A possible response to global warming. *Geophysical Research Letters*, 39: L09701. http://dx.doi.org/10.1029/2012GL051155.